AIMS Geosciences

AIMS Geosciences, 8(3): 326–345.
DOI: 10.3934/geosci.2022019
Received: 21 March 2022
Revised: 21 April 2022
Accepted: 26 April 2022
Published: 06 May 2022

http://www.aimspress.com/journal/geosciences

Research article

Impact of the closure of a coal district on the environmental issue of long-term surface movements

Andre Vervoort*

Department of Civil Engineering, KU Leuven, Leuven, Belgium

* **Correspondence:** Email: andre.vervoort@kuleuven.be; Tel: +3216321171.

Abstract: The environmental impact of deep underground coal mines using the longwall mining method is diverse, e.g., short- and long-term subsidence, damage to surface infrastructure, disturbance of the hydrogeological conditions, and the quality of groundwater and surface water. The study presented focusses on the long-term surface movements after the closure of an entire coal district. Due to the flooding of the underground infrastructure and rock mass, an upward surface movement or uplift is observed. For a specific site in the Campine coal district, Belgium results are presented of satellite data (radar-interferometry). However, the main aim of the study is to better understand the process of uplift and to determine the various mechanisms that are involved. For this purpose, an analytical framework was developed recently, and it was applied successfully in a relatively easy case. The case study of the paper is more challenging, but the usefulness of the analytical framework is clearly confirmed. The most important conclusions are that (i) the uplift is induced by an increase in water pressure after the closure, i.e., re-establishing the original hydraulic gradient, (ii) the expansion of both the goaf volumes and the volumes of the non-collapsed rock mass must be considered, and (iii) the assumption of a linear decrease of water pressure variation from the top to the bottom of the mined area at the end of the mining phase provides the most realistic results. However, the next step in the analysis should focus on a more advanced hydrogeological model of the complex underground environment.

Keywords: longwall mining; ground control; radar-interferometry; surface movement; uplift; estimation; analytical model

1. Introduction

The impact of the total extraction method of coal longwall mining on subsidence is well known [1–4]. One of the environmental issues linked to subsidence is the damage to buildings, roads, railway lines, pylons, and other infrastructure [3,5–8]. If the coal seams are situated at shallow depth, the infrastructure is sometimes abandoned, e.g., a parallel temporary road, situated outside the influence zone, is constructed, and used during the mining phase. Another example is that people are moved out of their houses during the mining phase. For deep coal mining, these actions are less frequently imposed. However, this does not mean that no damage is induced. In Figure 1, some examples above the Campine coal district, Belgium are shown of mining induced damage in buildings during the subsidence phase. Another environmental issue of subsidence is the impact on the hydrogeological context and on the quality of the surface water and groundwater [9–12]. In the Campine coal district, metre-scale subsidence occurred over areas of several 10 to 100 km². Part of these areas would be flooded, except if one permanently pumps the surface water and shallow groundwater away [13]. Natural waterways and canals need special attention when they cross such subsided areas, e.g., dikes must be constructed to restrain the water.

Figure 1. Some examples in the Campine coal district, Belgium of mining induced damage in masonry during the subsidence phase.

Although the largest surface movements occur during the active mining phase, one should not neglect the long-term surface movements. After mining, subsidence still occurs over very long time periods [14–16]. This movement often is not analyzed, as the monitoring of surface movements stops

a few years after mining. The most frequently used criterium to stop monitoring is the comparison of the additional movement recorded to the accuracy of the measuring technique. This criterium often has led to wrong conclusions on how long surface movement lasts after mining, i.e., one assumes that the subsidence did not last longer than a few years. During the past decades, remote sensing data by satellite images became available. The main advantages of these datasets are that they cover long time periods and large areas, and that their recording is independent of the mine operators. So, the surface movement over many years after mining can be analyzed. Such an analysis for the Campine coal district, Belgium showed that subsidence was still observed several decades after the end of mining in the vicinity of the recorded datapoints [15]. "Vicinity" was defined as a distance of ±1 km to the north and to the south, i.e., a distance larger than the depth of mining.

The same remote sensing data also allowed to characterize a relatively new phenomenon of surface movement, i.e., the upward movement or uplift. It clearly is linked to the flooding of the deep underground coal mines after their closure and the dismantling of the underground pumping installations. This phenomenon has been observed in several European coal districts, but also outside Europe. For the Campine coal district, Belgium the phenomenon has been intensively studied by using satellite data (radar-interferometry or InSAR (interferometry with synthetic aperture radar)). The European C-band ERS1/2 and ENVISAT-ASAR satellite images were made available for research through a research proposal of the European Space Agency (ESA) [17]. The various studies for the Campine coal district, Belgium can be summarized in a simplified and general way as follows ([13] and the references in that reference):

• The upward movement starts from a few years to about 10 years after the closure of the underground mine.

• The mines were closed in the period between 1988 and 1992, and now 30 years or more later, the phenomenon is still observed.

• The final cumulative amount of uplift will most likely be about an order of magnitude smaller than the total amount of subsidence. Overall, the subsidence is several meters (sometimes more than 10 m), while the uplift will be most likely be several decimeters to maybe a meter.

• However, there is no fixed ratio between total uplift vs. total subsidence for individual locations [16]. In other words, the uplift is not a simple rebound of part of the subsidence, i.e., the largest uplift values are not necessarily occurring where the largest subsidence took place.

• The rate of movement for the residual subsidence is the same order as the uplift rate, but again not location per location. In general terms, one is looking at mm- to cm-movements a year.

• Overall, the uplift is characterized by a large time dependent and spatial variation. However, the uplift values are distributed very heterogeneously over the mined and neighboring area. Uplift is observed at distances equal to several times the depth away from the mined zone.

• The first signs of uplift are mostly observed in the central mining part and, as a function of time, it spreads to the boundaries of the mined area and beyond.

• When looking at transects, e.g., in the north-south direction, the shape of the curves for the (residual) subsidence and for the uplift are different. This is a direct consequence of the earlier mentioned finding, i.e., the largest uplift values are not necessarily occurring where the largest subsidence took place.

As the uplift is not a simple rebound of the subsidence, different stresses and strains are induced, e.g., in buildings, during the subsidence phase and the uplift phase. This means that the orientation of the induced principal stresses and strains can be different between the subsidence and uplift phases.

The sign of loading also can be different. For example, a building that underwent a horizontal extension during subsidence can undergo a horizontal compression during uplift, or vice versa. Therefore, new or additional damage can be induced in infrastructure during the uplift phase, even that overall, the amount of total uplift is smaller than the total amount of subsidence. One should not forget that the infrastructure has already undergone a significant amount of loading during the mining phase. This maybe has not led to macro-fractures or visible damage, but there is certainly a build-up of induced stresses and strains in the construction, and most likely a minimum of micro-fracturing or -damage. The additional loading during the uplift phase must be added to the stresses and strains, induced by the subsidence phase. In other words, the superposition principles must be applied. Again, the importance must be pointed out that the uplift is not a simple rebound of part of the earlier subsidence. In literature, examples are given of damage during the uplift phase [18,19]. In Figure 2, some examples are presented of damage in masonry, observed during the uplift phase above the coal mine of Eisden, Belgium. These examples are situated in the zone studied further in the paper. The damage was not visible during the subsidence period, but as mentioned above these buildings have undergone the loading due to the subsidence.

2. Scope of research

The research focusses on the surface movement after closure above the various coal mines of the Campine basin in the north-east of Belgium. During the past years the phenomenon of uplift was investigated based on two series of InSAR satellite data, covering the periods from August 1992 through December 2000 (European C-band ERS1/2 data), and from December 2003 through October 2010 (ENVISAT-ASAR data). These data were extensively analyzed and showed that the phenomenon of uplift is a very complex process [13]. A link with the flooding of the underground was clearly established by others in different European coal districts [19–23]. However, many unknowns remained on the various mechanisms that induce uplift. Therefore, an analytical framework was developed to calculate the impact of various scenarios and assumptions. This helped to better understand the phenomenon. First, a relatively easy case was studied, providing satisfactorily results [24]. Second, more complex mining geometries are being studied. The main aim of these additional calculations remains to better understand the phenomenon and to investigate if the analytical framework needs to be further adapted or not. In [25,26], a transect was studied covering two coal mines, i.e., one closed in 1988 and the other already in 1966. The latter was partly flooded after the closure in 1966.

In this paper, a transect is investigated, which is situated close to the eastern end of the Campine coal basin. The mining geometry along this transect also is more complex than in the first study. The mined longwall panels in the Campine coal basin forms a narrow east-west band with normally a north-south width between 5 to 10 km and a total east-west length of about 60 km. This narrow band allows a 2D approach and the calculations are conducted along north-south transects. In this paper, the transect studied covers a north-south width of mined panels of 3.5 km.

Figure 2. Some examples of post-mining induced damage in masonry during the uplift phase. All examples are situated within the study area of this paper (coal mine of Eisden, Belgium).

3. Uplift measurements

Figure 3 illustrates well the complexity of the mining geometry with many superimposed longwall panels and multiple faults. It represents part of the coal mine of Eisden, Belgium. The blue enveloping line presents an approximate contour around these panels. The north-south transect studied in this paper is situated at an east-west coordinate of 0.0 km. The north-south width of the mined zone along this transect is 3.5 km (from 0.0 to 3.5 km). The mineable seams belong to the stratigraphical units of Westphalian A, B, and C [13]. On average, the mining height was composed of 85% coal and 15% of thin layers of waste rock. Shale, siltstone, sandstone, and thin (unmined) coal layers were observed between the mined coal seams. Overall, the successive strata were relatively thin (on the order of decimetres to 10-metres in scale). The overburden has a thickness of 350 to 475 m and is composed of Quaternary deposits (mainly sand, gravel, and loam), Neogene and Paleogene units (mainly sand, marl, and clay), and Cretaceous deposits (mainly calcarenite, chalk and marl, with a limited thickness of sand and clay at the bottom) [13]. Over the entire overburden, several aquifers and aquitards are present at different depths. The east limit of the concession of Eisden borders the Meuse river. In Figure 4, information on the mined panels along this transect are provided. Figure 4a presents the depth position of the various panels. A discretization in elements with a north-south length of 250 m is applied, as this is the size of the individual elements in the analytical model. The dip of the strata towards the north is visible. For example, the deepest panel is situated at the southern limit at a depth of −640 m and at the northern limit at a depth of −867 m. The

shallowest panel is over the first km situated at a depth of −381 m and at the northern limit at −590 m. Between the coordinates 2.25–3.00 km no mining took place underneath this transect. More to the east, panels were mined, but not to the west (see Figure 3). For north-south coordinate values less than 0 km, mining took place west of the transect line (up to a north-south coordinate of −1.5 km). In the southern half of the mined area along the transect the mining is more extensive, i.e., between the coordinates 0.25–1.75 km, the sums of the mining height of the various longwall panels are more than 5 m (Figure 4b). The maximum total mining height is situated at 1.125 km (sum equals to 10.9 m).

The transect studied in [13,24] was situated at an east-west coordinate of −2.5 km for the scale of Figure 3. The mine of Eisden was producing coal between 1922 and 1987. In 1988, access to the underground infrastructure was sealed off. In [13], more details are given about this mine and its geological context.

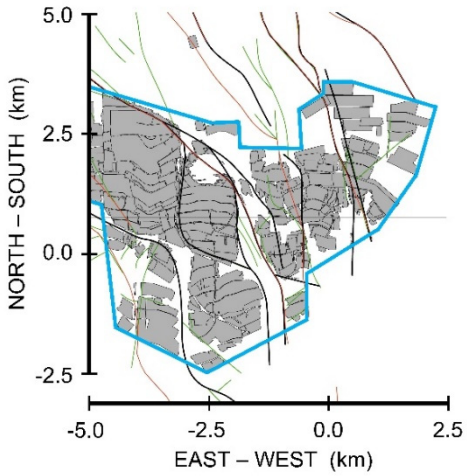

Figure 3. View on superimposed longwall panels, mined in the mine of Eisden, Belgium (based on [13]). The blue enveloping line presents an approximate contour around these panels. North-south transect studied in paper is situated at an east-west coordinate of 0.0 km.

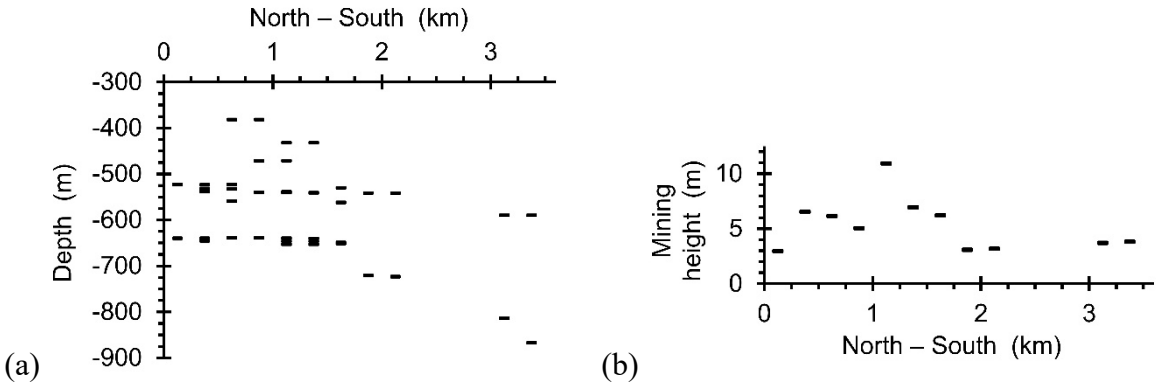

Figure 4. Mining characteristics along the north-south transect studied (east-west coordinate of 0.0 km in Figure 3): (a) Depth of the longwall panels; (b) total mining height.

The spatial distribution of surface movement for a 5-year period (i.e., period from December 1995 through December 2000) above and around the coal mine of Eisden is presented in Figure 5 (based on [13]). All recorded reflectors are divided in two groups. A first group represents the reflectors with a significant amount of uplift, i.e., with an average uplift rate over the 5-year period of more than 1 mm/year (Figure 5a). The second group represents reflectors with a residual subsidence of less than −1 mm/year, or with an average annual rate of ±1 mm/year, i.e., the often-assumed accuracy of the monitoring method over long time periods (Figure 5b). The latter spatial distribution clearly shows that within the mined area (blue enveloping line) no reflectors are observed that undergo a small surface movement or subsidence. Except for a few data points, this second group of movement types is situated 2 km or more away from the mined area. For a maximum depth of about −650 m (in the southern part) to −875 m (close to the northern limit), this means a distance—depth ratio of more than 2 to 3. For the measurements prior to 1995, these types of movement rates are closer to the mined area, but not within the mined area [13].

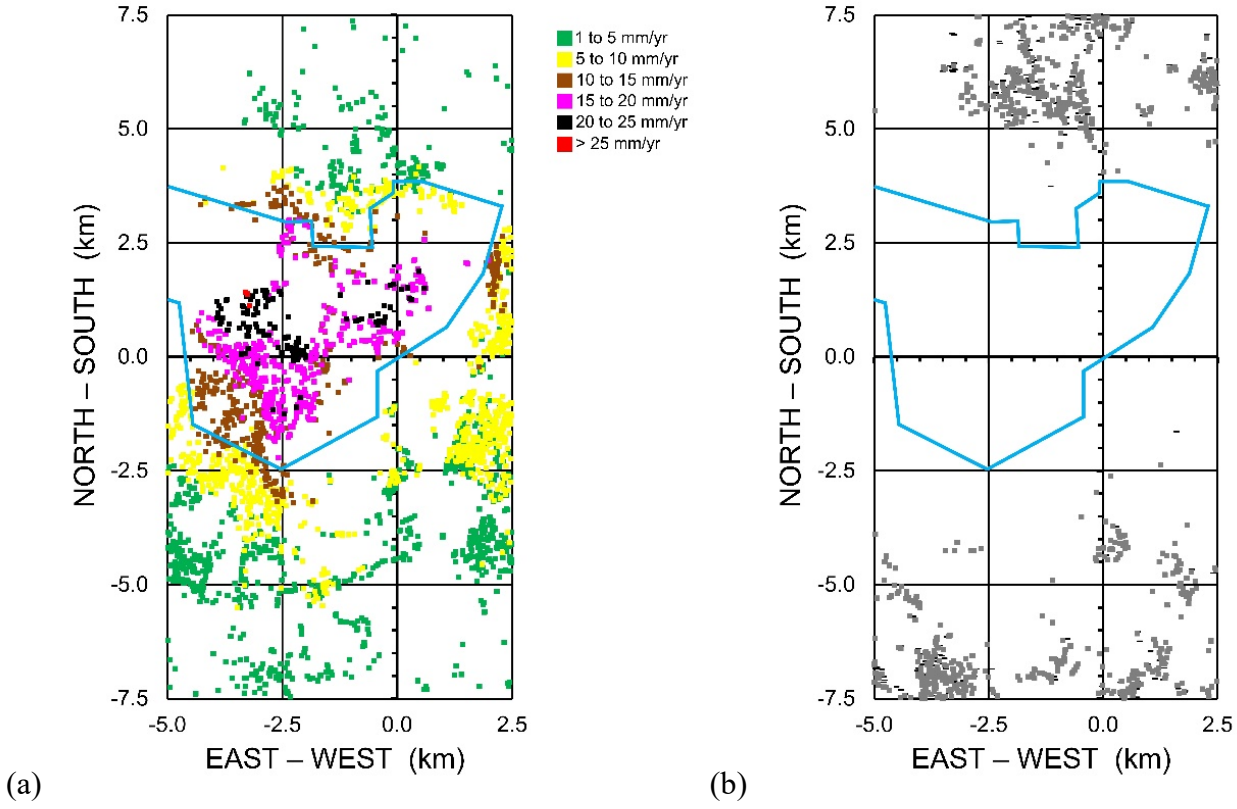

Figure 5. Spatial distribution of surface movement for a 5-year period (i.e., period from December 1995 through December 2000) above and around the coal mine of Eisden, Belgium (based on [13]): (a) additional uplift, corresponding to a rate larger than 1 mm/year; (b) residual subsidence corresponding to a rate larger than −1 mm/year (minus signs) or a movement with a rate of ±1 mm/year (grey blocks). Blue enveloping line presents the contour around the mined longwall panels.

Figure 5a clearly shows that away from the mined zone, i.e., at distances larger than 2 km, reflectors are also observed undergoing clear uplift (green color with average annual rates between 1 to

5 mm). Around the mine limits, these rates are mainly situated between 5 and 15 mm/year (yellow and brown color). In the more central zone, the average rates go as high as 25 mm/year (purple and black color) and for some reflectors even above (red color). A more detailed analysis and discussion of the spatial distributions of average rates are provided in [13], also including two other time periods.

As mentioned above, the analytical calculations are conducted for 2D-transects and their main purpose is to try to understand the various mechanisms involved in the uplift process and to quantify the impact of different parameters. Figure 6 presents the north-south transect for an east-west coordinate equal to 0.0 km. The individual reflectors within an east-west width of 750 m are presented for the two InSAR datasets, i.e., from August 1992 through December 2000 (European C-band ERS1/2 data; Figure 6a) and from December 2003 through October 2010 (ENVISAT-ASAR data; Figure 6b). The total amount of uplift, occurring during each period, is presented. If at least five reflectors are present in a 250-m interval, the average value of the intervals is calculated and presented by triangles.

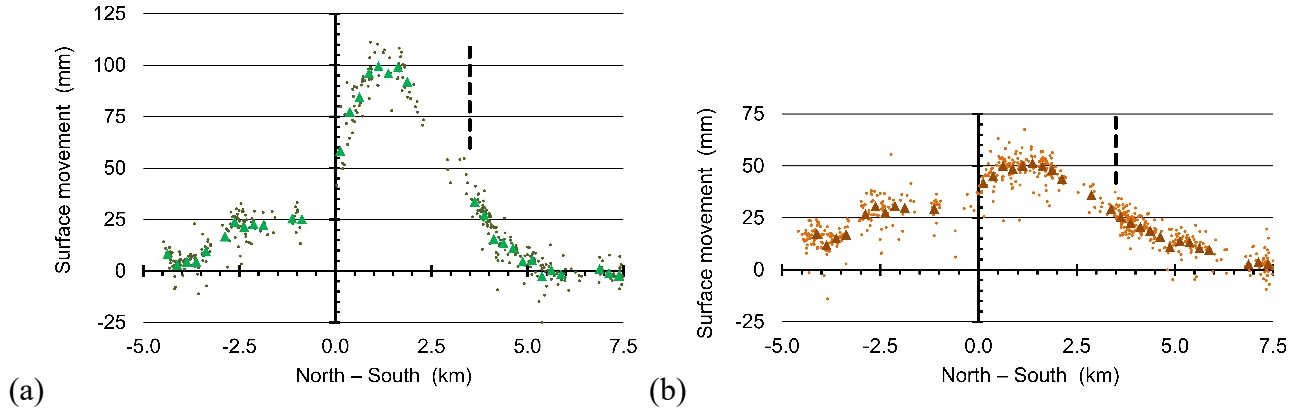

Figure 6. Surface movement along the 12.5-km long north-south transect at an east-west coordinate of 0.0 km of all reflectors within an east-west width of 750 m for the two InSAR datasets: (a) from August 1992 through December 2000 (European C-band ERS1/2 data); (b) from December 2003 through October 2010 (ENVISAT-ASAR data). The values for the individual reflectors are presented by dots and the average values over 250-m intervals by triangles (if at least five reflectors are present in the interval). The northern limit of the mined area is indicated by black dashed line at 3.5 km (southern limit corresponds to 0.0 km along this transect).

As is typical for the Campine coal district [13,16,27,28], an inverse trough shape curve is observed. The largest values are situated at north-south coordinates from 0.75 km to 1.75 km for the first observation period (Figure 6a) and from 0.5 km to 2.0 km for the second period. For both periods, the maximum per period is about 100 mm (average maxima between 97 mm and 101 mm) and about 50 mm (average maxima between 48 mm and 51 mm), respectively. Note that the second observation period is shorter than the first. Within the mined zone (north-south coordinates 0.0 to 3.5 km), the largest uplift values are observed. However, outside the mined zone, the uplift values are still significant. As mentioned earlier, to the west of the central transect for north-south coordinates from 0.0 to −1.5 km, some panels were mined (Figure 3). This is most likely an explanation for the plateau in uplift values, south of the mined limit. The spreading of the uplift over time is also visible when

comparing both transects. To the south of the mined zone, the average uplift is about one fourth of the maximum uplift in the first observation period and more than half in the second period. The extent of uplift, north of the mined zone, is up to a north-south coordinate of about 5 km in the first time period and up to about 7 km for the second period. So, the uplift clearly spreads out over time.

Around north-south coordinates between 0.0 km and −0.75 km, and between 2.0 km and 3.25 km, no or very few reflectors are identified.

4. Presentation of analytical framework

The proposed analytical framework with the aim to get a better understanding of the process of uplift was first presented in [24]. For more detailed information and background, the reader is referred to that paper. However, the most relevant aspects are summarized below, and in Figure 7.

During the mining phase, drainage occurs, resulting in a lower hydraulic pressure. After mine closure, the hydraulic pressure is increased again up to the original hydraulic gradient. An increase in pore pressure leads first to an expansion of the in-situ rock material, and this expansion is transferred to the surface. The analytical model considers drainage in both the goaf volumes and the strata surrounding them, i.e., the non-collapsed rock mass. For the mined zone, satisfactorily results were obtained in earlier analysis when an enveloping line was drawn around all longwall panels [24,26]. In Figure 7a, a first enveloping line is drawn in blue covering the north-south coordinates 0.0–3.5 km. However, by considering a drained zone only in the mined area, the uplift outside the mined zone was underestimated [24,26]. Therefore, the drained zone was extended over 1 km to both the north and the south. For the transect studied in this paper, longwall panels were also mined to the west of the central transect over north-south coordinates of 0.0 to −1.5 km (see Figure 3). Hence, the drained zone is extended over 2.5 km (1.5 km + 1 km), south of the mined limit along the central transect. This extension is drawn by a purple dashed line in Figure 7a.

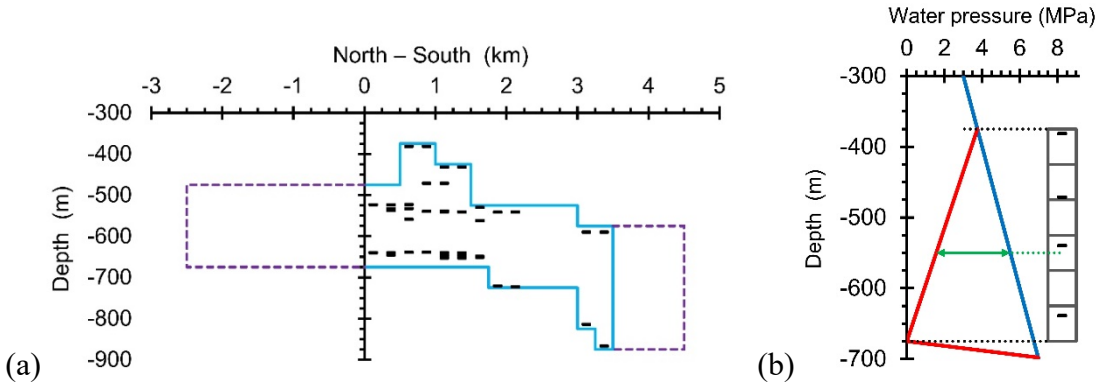

Figure 7. Illustration of the drained zone at the end of the mining phase. (a) Along the 2D north-south transect, two closed enveloping lines (in blue and in purple) are drawn around the longwall panels (Figure 4a), representing the area with a lower hydraulic pressure at the end of the mining phase; (b) Illustration of change in water pressure for the fourth column of elements (0.75–1.0 km), with in blue, the original (and final) hydrostatic gradient and in red, the lower water pressure at the end of the mining phase.

In the analytical framework, it is not assumed that full drainage (i.e., zero water pressure) occurred over the entire height of the drained strata. A linear decrease of the average water pressure from the top to the bottom of the mined area is assumed. This is illustrated in Figure 7b for an example, i.e., the fourth column of elements between north-south coordinated 0.75–1.0 km. At the top, it is assumed that the original hydraulic pressure already has been re-established at the end of the mining phase. At the bottom, where the most recent mining took place, the water pressure is assumed to be zero. For the fourth column of elements (0.75–1.0 km), the initial (and final) hydraulic pressure at top and bottom was 3.75 MPa and 6.75 MPa, respectively (blue line). At the end of the mining phase, the average water pressure varies between 3.75 MPa and 0.0 MPa (red line). For each depth, the difference between both lines corresponds to the potential of water pressure increase (green arrow) after closure till a new equilibrium is reached. Note that the lines represent the average change as a function of depth and that the pore pressure in individual points varies around these average lines.

The north-south model is discretized in elements of 50 m (depth) on 250 m (N-S length). The expansion of each element takes place at the center of the element. The composition of each element (i.e., goaf volume vs. the non-collapsed strata) determines the average stiffness of the element, and thus the amount of expansion. The stiffness values for both materials are 0.2 and 2 GPa, respectively (Poisson's ratio equal to 0.25). This gives a ratio of 1 on 10. The goaf height is taken equal to four times the mining height. These assumptions resulted in satisfactorily correlations between measurements and calculations [24,26]. Physicochemical swelling of the clay minerals in a coal mine after flooding is not considered separately in the calculations. The main reason is that there are still many unknows. However, the impact of the physicochemical swelling could be incorporated by decreasing the stiffness of the mechanical swelling.

Two main criteria were used to evaluate the comparison: it is important that the calculated maximum uplift value is the correct order of magnitude, but even more important is that the shapes of the calculated and measured uplift curves along the north-south transects are similar. The latter is evaluated by presenting the curves as a percentage of their corresponding maximum value (see further). The evaluation of the absolute maximum uplift value is not straightforward, as the final in-situ uplift value is unknown. One can only estimate it, as the process of uplift still carries on. Most likely, along the transect studied the final maximum uplift will be situated between 0.3 m and 0.6 m.

In the fourth column of elements (Figure 7b), four longwall panels were mined between a depth of −381 m and −639 m. Taking the discretization into account, the top element starts at a depth of −375 m and the bottom element stops at a depth of −675 m. Four of these 6 elements contain a single longwall panel; the two remaining ones are only composed of non-collapsed strata. For example, the element situated between −525 m and −575 m is composed of 4.04 m goaf material (4 times the mining height of 1.01 m) and 45.96 m of non-collapsed material. The equivalent vertical stiffness of this element is equal to 1.16 GPa (50 m, divided by the sum of 45.96 m/2.0 GPa and 4.04 m/0.2 GPa). At its center, the change in water pressure is 3.94 MPa (difference between original/final water pressure at central depth of −550 m, i.e., 5.50 MPa, and reduced pressure of 1.56 MPa). The calculated underground expansion of this element is 85 mm. About 40 mm is due to the expansion of the goaf volume and about 45 mm due to the expansion of the non-collapsed strata. For this element, both contributions are similar, as the ratio of the height of both material types is also about 1 on 10 (similar, but the other way, as the stiffness). Based on the information for this element, one should not conclude that the contribution of both components is always the same. For example, for the elements below and above it, the contribution by the goaf volume is 0%, as no longwall panel is

present in these elements. On the other hand, for the element to the north (i.e., at 1.125 km and depth between −525 m and −575 m), the expansion of only the goaf volume is 149.5 mm, and it is 27.2 mm for the remaining non-collapsed strata. The height of each material type is 17.72 m (total mining height is 4.43 m) and 32.28 m, respectively.

A transfer function, based on the Boussinesq theory, translates the underground expansion into surface movement. Directly above the center of the element taken as example (i.e., at 0.875 km), its contribution to the uplift of the surface node is about 21 mm. For the surface nodes at distances of 750 m to the north and to the south, the surface nodes move about 3.2 mm due to the expansion of that single element. Similar calculations are conducted for all underground elements in the drained area. The final or total uplift of a surface node is the sum of the contributions from all elements within its zone of influence. The contribution of a single element is relatively small. For the basic assumptions the total uplift at a north-south coordinate of 0.875 km is 442 mm (see further).

5. Results of the analytical calculations

5.1. Approach and assumptions, based on [24]

The analytical calculations along the north-south transect are compared to the two datasets of the InSAR-observations. The increase in uplift over the entire observation period is considered, and a comparison is made with the individual measurements (i.e., individual dots in Figure 6). As mentioned above, the main criterium to evaluate the analytical framework is the shape of the uplift curve along the transect. Therefore, the data are presented as a percentage of the maximum value. For the calculations, the maximum is well defined, i.e., the largest calculated uplift of all surface nodes, situated at a 250-m spacing. For the measurements, the largest average uplift over 250-m intervals is used. Hence, some individual measurements have a relative uplift value larger than 100%. In second instance, the absolute uplift values are evaluated, but the aim is only to obtain the correct order of magnitude. The reason for this is that the final cumulative uplift is unknown. Also, if the shape is acceptable, the calculated absolute value can be changed easily, by changing the parameters values. Thereby, it is important that the various ratios remain the same. For example, by increasing the stiffness values of both material types with 10%, the uplift values are decreased by 10% (and vice versa).

Two basic scenarios are considered: only the strata within the mined area are drained at the end of the mining phase (blue enveloping line in Figure 7a), and the situation whereby the strata to the south and the north are also drained (purple enveloping line in Figure 7a). Figure 8 presents the four combinations, i.e., the two datasets and the two scenarios. The same colors are used as in Figures 6 and 7. As mentioned earlier, one observes above the Campine coal mines that as a function of time the uplift spreads from the central area to the mine borders and beyond. This would mean that the increase in water pressure at the beginning of the uplift process is mainly concentrated in the drained mined area (blue enveloping line), and that at a later phase the water pressure also starts to increase in the extended drained zone. Unfortunately, no data is available for the Campine coal basin on the evolution of the water pressure as a function of time and spatial coordinates.

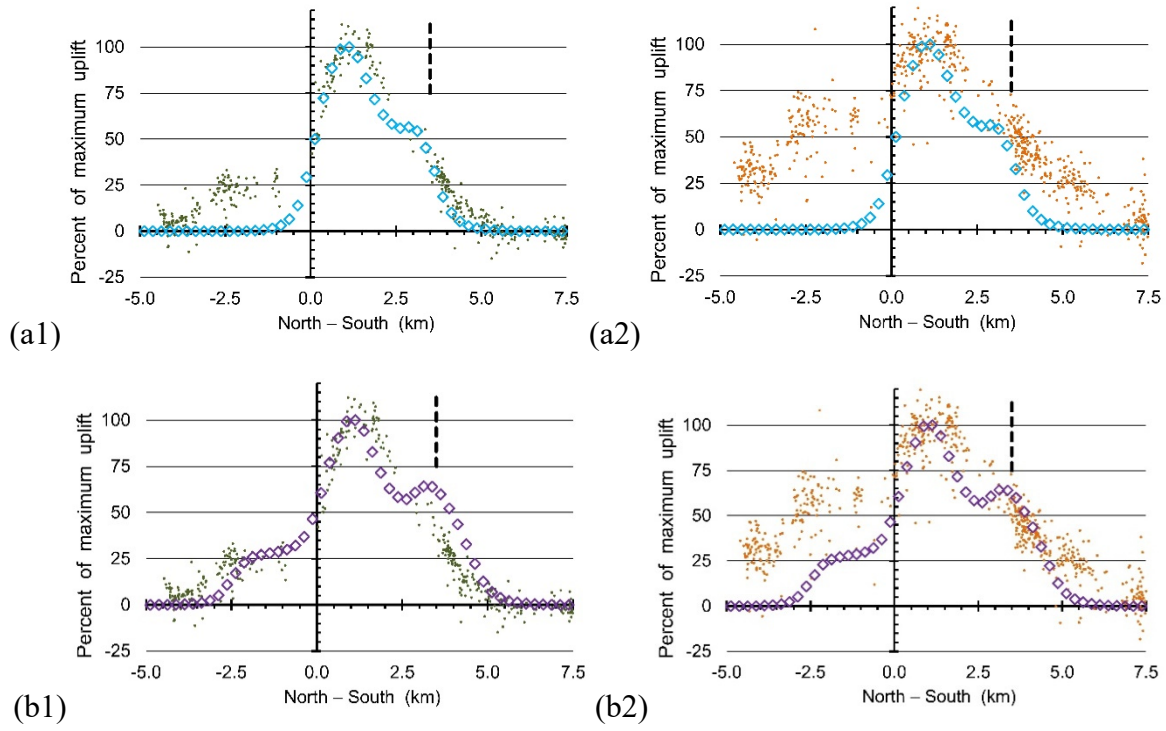

Figure 8. Comparison between the individual measured values, presented by green (left column) and brown (right column) dots (from August 1992 through December 2000 (European C-band ERS1/2 data) and from December 2003 through October 2010 (ENVISAT-ASAR data), respectively), and calculated uplift values, presented by blue (top row) and purple (bottom row) diamonds (for the blue and purple enveloping lines in Figure 7a, respectively). All data are presented as a percentage of their corresponding maximum value.

Looking at the mined area for north-south coordinates 0.0–3.5 km, the calculated values for both scenarios are relatively close to the individual data points of both observation periods. The maximum calculated values are situated around 1 km (between 0.75 km and 1.25 km). In the first observation period, the larger measured values are observed at coordinate values of 0.75 km to 1.75 km. In the second period, this width is slightly larger, i.e., between 0.5 km and 2.0 km. Between the southern limit of mining and the maximum area, the correlation with the observations is more than satisfactorily. North of the maximum, the calculations clearly show a clear dip in the curve around 2.5 to 3.0 km. The reason for it is the absence of mining between 2.25 and 3.0 km. Unfortunately, no to very few reflectors are available within this zone. So, it is difficult to conclude if the calculations confirm the observations. North of the mined area, the limited drained area results in a good correlation with the data of the first time period (Figure 8a1) and the extended drained area results in a good correlation for the second period (Figure 8b2), at least over a distance of 1.5 km. More to the north, i.e., for coordinate values larger than 5 km, there is still an underestimation. This is further discussed in the paragraph "Discussion and conclusions". The other two combinations result, north of the mined limit, in an underestimation (Figure 8a2) and an overestimation (Figure 8b1) of the measured values. South of the mined limit, the presence close to the west of the central transect line of mined panels has a significant effect. Re-establishing the water pressure in the mined area only

does not give acceptable results. For both observation periods, the uplift is heavily underestimated for negative coordinate values. By extending the drained zone over 2.5 km to the south, the increase of water pressure leads to a good correlation over this distance in the first observation period (Figure 8b1). The large uplift values in the second observation period, i.e., 50 to 70% of the maximum average value, are not confirmed by the models. (See also paragraph "Discussion and conclusions")

The total calculated uplift is composed of three components: the expansion of the goaf volume, the expansion of the non-collapsed strata within the mined area, and the expansion of the strata below the mined area. For the latter, a thickness of 25 m is assumed [24]. Its contribution to the total uplift is very small. The maximum total calculated uplift is 447 mm and 450 mm, for blue and purple scenarios (Figure 7a), respectively. These values fit well into the range of expected maximum uplift, once an equilibrium will be reached. As mentioned above, the expected range is 0.3 m to 0.6 m. In other words, the chosen parameters values in [24] are again confirmed to be realistic values. In [24], the various values were not determined by back-analysis; rather, these values were determined by following logical reasoning and a verification afterwards whether a reasonable match is observed.

At first glance, the shapes of the curve of the absolute total uplift by the three components (purple scenario) and of the curve corresponding to the goaf expansion only might seem to be similar, but that is not the case (Figure 9). For the expansion of only the goaf volumes, there is, logically, no expansion of the strata outside the mined area (to the north and to the south). On the other hand, the maximum uplift is for both curves situated at the same north-south coordinate, i.e., around 1.125 km. The dip around 2.625 km is also present in both curves. However, the ratio between the uplift value at a certain position and the maximum is mostly smaller for the goaf contribution only. For example, for the dip location (at 2.625 km), the ratio for goaf volume only is 21% (52 mm vs. maximum of 246 mm) and for all contributions the ratio is 57% (257 mm vs. 450 mm). Looking at the values at the borders of the mined zone, the ratios at the southern border (0.125 km) are 45% (goaf only, 111/246 mm) and 61% (all components, 273/450 mm), and, at the northern border (3.375 km), 22% (goaf only, 55/246 mm) and 64% (all contributions, 288/450 mm).

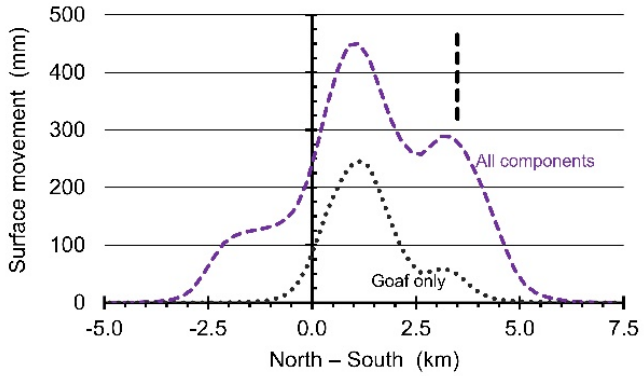

Figure 9. Absolute calculated uplift along the north-south transect for the extended drained zone (purple enveloping line in Figure 7a). Both the sum of all three components (purple dashed line) and of the goaf volume only (grey dotted line) are presented.

In Figure 10, the relative curve of the goaf contribution only is plotted on top of the relative measured values for both periods. These curves confirm earlier findings, i.e., considering the

expansion of the goaf volumes only cannot result in a satisfactorily correlation. The fact that the maximum value occurs at the correct north-south coordinate does not change this conclusion.

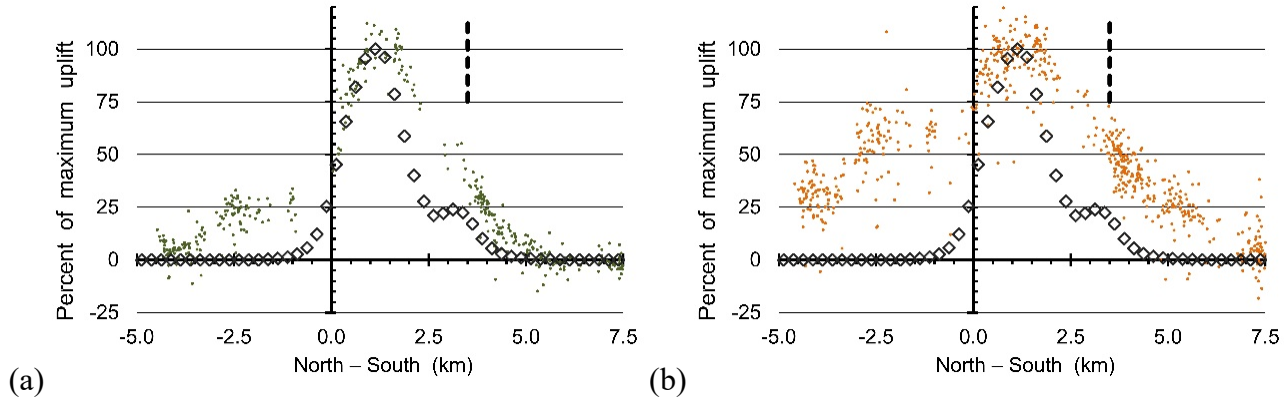

Figure 10. Comparison between the individual measured values and calculated uplift values for the expansion of the goaf volumes only (grey diamonds): (a) first observation period (green dots, from August 1992 through December 2000 (European C-band ERS1/2 data)); (b) second observation period (brown dots, from December 2003 through October 2010 (ENVISAT-ASAR data)). All data are presented as a percentage of their corresponding maximum value.

5.2. Impact of assuming an open reservoir

Figure 7b illustrates the water pressure distribution along a vertical line at the end of the mining phase, i.e., the distribution assumed in the basic analytical framework [24]. The linear decrease from top to bottom is based on measurements conducted in other coal districts [29–31]. This assumption provides realistic results and more than acceptable correlations with the measurements. It is also assumed that the linear variation remains during the increase of the water pressure after closure. Therefore, the shape of the calculated curves of the relative uplift values does not change over time. However, Figure 6 clearly shows an evolution as a function of time, i.e., a change between the first and the second observation period. Rather, this is explained by an extension of the north-south width where the increase in water pressure starts, than that the linear trend needs further adaption. Of course, the hydrogeological context is complex and detailed measuring campaigns are needed to better define the hydrological parameters values and their variation as a function of time and of spatial coordinates.

Other scenarios are certainly possible and should be evaluated. The advantage of the analytical framework is that one can analyze different scenarios in a quick and easy way. Plus, one can analyze the impact by only changing one aspect of the model. Another scenario is presented by [32,33]. I interpret their approach as that they first assume that the entire coal strata are completely drained at the end of the mining phase, i.e., a zero-water pressure. Second, they assume that the fully drained underground rock mass is filled over time with water like an open reservoir, i.e., from bottom to top. Third, they consider two possibilities, one, whereby the vertical columns are connected, and a second, whereby the vertical columns are independent of each other. For the connected columns, I have translated this in the analytical framework, as that first the bottom part between a depth of, e.g., from

−857 m to −775 m is filled with water. This means only the part north of the 3-km coordinate. This is followed by an increase in water level between, e.g., −875 m and −675 m (so, north of 1.75 km), and so on. The last step would be that, at the north-south coordinate equal to 3.375 km, the water pressure has reached 8.75 MPa at the depth of −875 m. For the independent columns, I have assumed that, at the start of the filling process, the water level increases over, e.g., 100 m in the various columns from the bottom of the drained area. However, only columns with longwall panels are considered. In a second step, an additional 100 m is further filled, and so on.

In Figures 11 and 12, the results for these two alternative scenarios are presented. Apart from the hydrological situation at the end of the mining phase, i.e., a zero-water pressure in the drained area, and the way that the drained area is filled with water, i.e., like an open reservoir, all other assumptions and parameter values are the same as in the basic framework, presented above.

The variation in shape of the cumulative uplift curves as a function of the water pressure is for the dependent or connected columns significant (Figure 11a). For low water pressure values, the uplift is situated in the northern part of the mined area, i.e., the deepest part of the mine. The maximum of the curves moves slowly more to the south, as the water pressure increases. For 6 and 8 MPa water pressure (at 3.375 km), the maximum cumulative uplift is situated at a north-south coordinate equal to 1.125 km. For 4 and 2 MPa, the maximum is situated at 3.125 km. In none of the north-south transects, this change in uplift curve was ever observed in the Campine coal district [13,16,27,28]. For a water pressure equal to 8 MPa at the bottom (a depth of −875 m), the calculated value at 3.375 km (northern limit of the mined area) is equal to 305 mm. This value corresponds to 51% of the maximum calculated value (i.e., 600 mm).

The variation in shape of the cumulative uplift curves as a function of the water pressure is for the independent columns smaller (Figure 11b). The maximum of the four cumulative curves presented are 31 mm (for 1 MPa), 106 mm (2 MPa), 342 mm (4 MPa) and 592 mm (6 MPa), respectively. The maxima for the two lowest values are situated at a coordinate of 1.375 km and for the two largest at 1.125 km. In the northern part of the mined area, the measured uplift is significantly underestimated.

Several researchers have monitored the relation between the increase in water pressure and the uplift. They observed a linear trend, e.g., [21]. Of course, the water pressure does not necessarily increase linearly as a function of time. As discussed above, for the basic framework assumptions, such a linear correlation between both parameters is valid. In Figure 12, the calculated cumulative uplift for both sets of assumptions (i.e., an open reservoir with connected and independent columns, respectively) are presented as a function of the water pressure increase. Data for four locations are presented. All curves are non-linear for the first half of the water level increase. Afterwards the variations become linear.

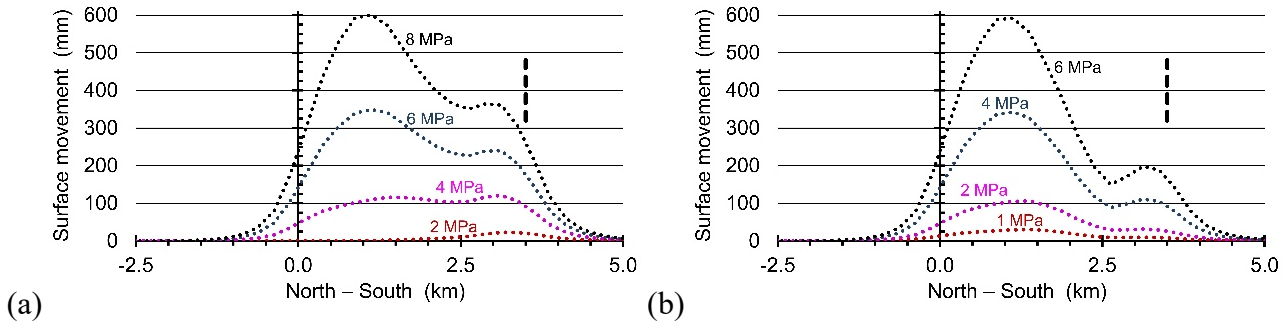

Figure 11. Calculated cumulative uplift curves along the north-south transect as a function of the increase in water pressure at the bottom of the drained area, assuming a zero-water pressure at the end of the mining phase and the filling of the drained area like the filling of an open reservoir: (a) Connected columns; (b) Independent columns. (See text for more detailed description.)

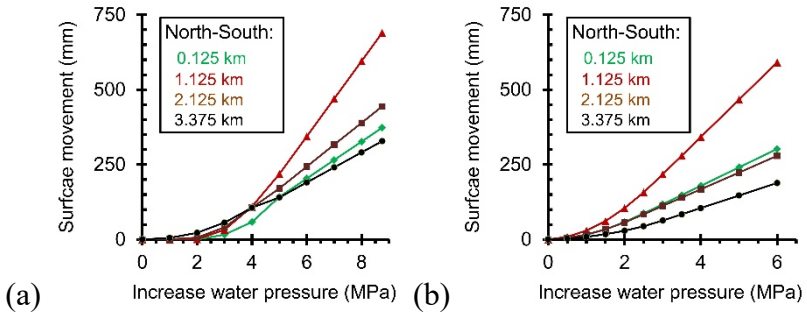

Figure 12. Calculated cumulative uplift at four locations as a function of the increase in water pressure at the bottom of the drained area, assuming a zero-water pressure at the end of the mining phase and the filling of the drained area like the filling of an open reservoir: (a) Connected columns; (b) Independent columns. (See text for more detailed description.)

6. Discussion and conclusions

The main aim of the study is to improve our knowledge about the mechanisms involved in the process of surface uplift after the dismantling of the pumping stations, the closure of the underground access and the subsequent flooding of the underground infrastructure and rock mass. The study is based both on detailed measurements of surface movements over long time periods and large areas, and on the analysis of the phenomenon using an analytical framework. Over the past years, several studies were conducted above different closed mines of the Campine coal district, Belgium. In this study, a more complex mining geometry was chosen, so that all earlier observed findings could be evaluated on their merits. Like earlier studies, a 2D-approach was applied, i.e., a north-south transect.

The analysis of the satellite data (radar-interferometry or InSAR (interferometry with synthetic aperture radar)) confirms that the uplift curve along the north-south transect can be approximated by an inverse trough shape. The north-south length of the mined area along this transect is 3.5 km. The observed shape is not fully symmetrical. The largest values are situated over a relatively wide length

(i.e., at north-south coordinates from 0.75 km to 1.75 km for the first observation period, and from 0.5 km to 2.0 km for the second period). As for other coal mines in the Campine basin, the uplift spreads as a function of time from the central area to the mine borders and beyond. This would mean that the increase in water pressure at the beginning of the uplift process is mainly concentrated in the drained mined area (blue enveloping line in Figure 7a), and that at a later phase the water pressure also starts to increase in the extended drained zone. There is a significant variation in annual uplift rates. Around the mine limits, these rates are mainly situated between 5 and 15 mm/year. In the more central zone, the average rates go as high as 25 mm/year and for some reflectors even above. Within the mined area no reflectors are observed that undergo small surface movements (rates of ±1 mm/year) or subsidence. These types of movements are only observed at 2 km or more away from the mined area, which corresponds to a distance—depth ratio of more than 2 to 3.

Overall, the earlier developed analytical framework and basic assumptions for the various parameters values also result in satisfactorily correlations with the measured values. Note that the various values were not determined by back-analysis. Rather, these values were determined by following logical reasoning and a verification afterwards whether a reasonable match is observed [24]. There is no discussion that within the mined area the correlation is good. The maximum total calculated uplift is about 0.45 m. It fits well into the range of expected maximum uplift, once an equilibrium will be reached, i.e., a range between 0.3 m and 0.6 m. In other words, the chosen parameters values in [24] are again confirmed to be realistic values. The new case study also confirms that considering the expansion of the goaf volumes only cannot result in a satisfactorily correlation with the measurements. The fact that the maximum value occurs at the correct north-south coordinate does not change this finding.

Outside the mined area, the findings need to be nuanced, i.e., they need to be critically examined. In comparison to earlier studies, this is the most valuable contribution of the research presented in the paper. North of the mined area, a good correlation with the data is observed for the first time period without considering the expansion of the drained area to the north. A good correlation, at least over a north-south length of 1.5 km, is observed for the second period, if the drained area is extended over 1 km, north of the mined area. Further to the north, there is an underestimation. South of the mined limit, the presence of mined panels close to the west of the central transect line has a significant effect. Re-establishing the water pressure in the mined area only, i.e., from 0.0 km to 3.5 km, does not give acceptable results. For both observation periods, the uplift is heavily underestimated south of the mined limit. By extending the drained zone over 2.5 km to the south, the increase of water pressure leads to a good correlation over this distance in the first observation period. The large observed uplift values in the second observation period, i.e., 50 to 70% of the maximum average value, are not confirmed by the models.

The lack of knowledge of the hydrogeological conditions and of the evolution of the water pressure as a function of time and the spatial coordinates is an obstacle to the further improvement of the analytical model. Advanced hydrogeological modelling could help to learn more about the distribution of the water pressure at the end of the mining phase and, more specifically, the extent of the drained area. Now, this task should not be underestimated. The presence of many faults makes the task complex. Also, at a north-south coordinate of about −0.5 km, the river Meuse crosses the north-south transect.

Although the hydrogeological knowledge around the mined area needs further improvement, the assumed variation as a function of depth of the water pressure at the end of the mining phase seems

to be an acceptable assumption. A linear decrease of the average water pressure from the top to the bottom of the mined area is assumed. At the top, it is assumed that the original hydraulic pressure already has been re-established at the end of the mining phase. At the bottom, where the most recent mining took place, the water pressure is assumed to be zero. After mine closure, the water pressure increases systematically till the original hydraulic gradient is reached. Two alternatives to this linear variation are evaluated, but they do not provide acceptable results. The alternatives assume a zero-water pressure at the end of the mining phase and the filling of the drained area like the filling of an open reservoir, whereby the vertical columns are either connected with each other, or react independently of each other.

Conflict of interest

The author declares no conflict of interest.

References

1. Galvin JM (2016) *Ground engineering - Principles and practices for underground coal mining*. Springer International Publishing, Switzerland. https://doi.org/10.1007/978-3-319-25005-2
2. Peng SS (1992) *Surface subsidence engineering*. SME, New York, NY, USA.
3. Wagner H, Schümann HER (1991) Surface effects of total coal-seam extraction by underground mining methods. *J S Atr Inst Min Metall* 91: 221–231. https://hdl.handle.net/10520/AJA0038223X_2005
4. Whittaker BN, Reddish DJ (1989) *Subsidence: occurrence, prediction and control*. Elsevier, Amsterdam.
5. Chomacki L, Rusek J, Słowik L (2021) Selected artificial intelligence methods in the risk analysis of damage to masonry buildings subject to long-term underground mining exploitation. *Minerals* 11: 958. https://doi.org/10.3390/min11090958
6. Rusek J, Tajduś K, Firek K, et al. (2021) Score-based Bayesian belief network structure learning in damage risk modelling of mining areas building development. *J Cleaner Prod* 296: 126528. https://doi.org/10.1016/j.jclepro.2021.126528
7. Yang Z, Li Z, Zhu J, et al. (2018) An InSAR-based temporal probability integral method and its application for predicting mining-induced dynamic deformations and assessing progressive damage to surface buildings. *IEEE J Sel Top Appl Earth Obs Remote Sens* 11: 472–483. https://doi.org/10.1109/JSTARS.2018.2789341
8. Florkowska L (2013) Example building damage caused by mining exploitation in disturbed rock mass. *Stud Geotech Mech* 35: 19–38. https://doi.org/10.2478/sgem-2013-0021
9. Masood N, Hudson-Edwards K, Farooqi A (2020) True cost of coal: coal mining industry and its associated environmental impacts on water resource development. *J Sustainable Min* 19: Article 1. https://doi.org/10.46873/2300-3960.1012
10. Li Y, Peng SS, Zhang J (2015) Impact of longwall mining on groundwater above the longwall panel in shallow coal seams. *J Rock Mech Geotech Eng* 7: 298–305. https://doi.org/10.1016/j.jrmge.2015.03.007
11. Vitale A (2012) Surface water impact assessment of longwall mining subsidence. Engeny Water Management, Galilee Coal Project SEIS Technical Report.

12. TEC (2007) Impacts of longwall coal mining on the environment in New South Wales. *Total Environment Centre*, Sydney, Australia.
13. Vervoort A (2021) Uplift of the surface of the earth above abandoned coal mines. Part A: Analysis of satellite data related to the movement of the surface. *Int J Rock Mech Min Sci* 148: 104896. https://doi.org/10.1016/j.ijrmms.2021.104896
14. Tajduś K, Sroka A, Misa R, et al. (2021) Analysis of mining-induced delayed surface subsidence. *Minerals* 11: 1187. https://doi.org/10.3390/min11111187
15. Vervoort A (2020) The time duration of the effects of total extraction mining methods on surface movement. *Energies* 13: 4107. http://dx.doi.org/10.3390/en13164107
16. Vervoort A (2020) Long-term impact of coal mining on surface movement: residual subsidence versus uplift. *Min Rep Glückauf* 156: 136–141.
17. Devleeschouwer X, Declercq PY, Flamion B, et al. (2008) Uplift revealed by radar interferometry around Liège (Belgium): A relation with rising mining groundwater. In: *Proceedings of the symposium post-Mining 2008*, Nancy, France.
18. Dudek M, Rusek J, Tajduś K, et al. (2021) Analysis of steel industrial portal frame building subjected to loads resulting from land surface uplift following the closure of underground mines. *Arch Civ Eng* 67: 283–298. http://dx.doi.org/10.24425/ace.2021.138056
19. Baglikow V (2011) Damage-relevant effects of mine water recovery—Conclusions from the Erkelenz hard coal district. *Markscheidewesen* 118: 10–16.
20. Samsonov S, d'Oreye N, Smets B (2013) Ground deformation associated with post-mining activity at the French—German border revealed by novel InSAR time series method. *Int J Appl Earth Obs Geoinform* 23: 142–154. https://doi.org/10.1016/j.jag.2012.12.008
21. Caro Cuenca M, Hooper AJ, Hanssen RF (2013) Surface deformation induced by water influx in the abandoned coal mines in Limburg, the Netherlands observed by satellite radar interferometry. *J Appl Geophys* 88: 1–11. http://dx.doi.org/10.1016/ j.jappgeo.2012.10.003
22. Herrero C, Muñoz A, Catalina JC, et al. (2012) Prediction and monitoring of subsidence hazards above coal mines (Presidence). *RFCS Final Report RFCR-CT-2007-00004*, EUR 25057 EN. Brussels, Belgium: European Commission.
23. Bekendam RF, Pöttgens JJ (1995) Ground movements over the coal mines of southern Limburg, The Netherlands, and their relation to rising mine waters. In: *Proceedings of the Fifth International Symposium on Land Subsidence*, The Hague, the Netherlands, IAHS234: 3–12.
24. Vervoort A (2021) Uplift of the surface of the earth above abandoned coal mines. Part B: Framework to understand and explain uplift. *Int J Rock Mech Min Sci* 148: 104947. https://doi.org/10.1016/j.ijrmms.2021.104947
25. Vervoort A, Declercq PY (2017) Upwards surface movement above deep coal mines after closure and flooding of underground workings. In: *Proc. of 36th International Conference on Ground Control in Mining*. Morgantown, WV: West Virginia University, 329–336.
26. Vervoort A (2022) Upward surface movement above deep coal mines after closure and flooding: analytical modeling results. In: *Proc. of the SME 2022 International Conference on Ground Control in Mining*. Canonsburg PA, United States [in press].
27. Vervoort A (2016) Surface movement above an underground coal longwall mine after closure. *Nat Hazards Earth Syst Sci* 16: 2107–2121. https://doi.org/10.5194/nhess-16-2107-2016

28. Vervoort A, Declercq PY (2018) Upward surface movement above deep coal mines after closure and flooding of underground workings. *Int J Min Sci Technol* 28: 53–59. https://doi.org/10.1016/j.ijmst.2017.11.008
29. David K, Timms WA, Barbour SL, et al. (2017) Tracking changes in the specific storage of overburden rock during longwall coal mining. *J Hydrol* 553: 304–320. http://dx.doi.org/10.1016/j.jhydrol.2017.07.057
30. Tammetta P (2013) Estimation of the height of complete groundwater drainage above mined longwall panels. *Groundwater* 51: 723–734. https://doi.org/10.1111/gwat.12003
31. Tammetta P (2014) Author's Reply on Discussion. *Groundwater* 52: 339–342. https://doi.org/10.1111/gwat.12190_2
32. Zhao J, Konietzky H (2021) An overview on flooding induced uplift for abandoned coal mines. *Int J Rock Mech Min Sci* 148: 104955. https://doi.org/10.1016/j.ijrmms.2021.104955
33. Zhao J, Konietzky H, Herbst M, et al. (2021) Numerical simulation of flooding induced uplift for abandoned coal mines: simulation schemes and parameter sensitivity. *Int J Coal Sci Technol* 8: 1238–1249. https://doi.org/10.1007/s40789-021-00465-x

AIMS Press